All-Optical Scheme for Generation of Isolated Attosecond Electron Pulses

M. Kozák*
Faculty of Mathematics and Physics, Charles University, Ke Karlovu 3, 12116 Prague 2, Czech Republic

(Received 27 May 2019; published 13 November 2019)

We theoretically propose an all-optical scheme for generation of isolated electron pulses with subfemtosecond durations for ultrafast electron microscopy and diffraction. The scheme is based on simultaneous longitudinal and transverse momentum modulation of freely propagating electrons at two distinct frequencies via ponderomotive interaction with tailored light fields of three phase-controlled laser pulses in vacuum. After a drift distance, an attosecond electron pulse train is formed with the individual pulses displaced in the transverse direction. Spatial filtering of the electron beam by an aperture leads to isolation of an individual attosecond pulse with a duration of <100 as. Subfemtosecond isolated electron pulses will enable direct space-time imaging of attosecond electronic dynamics in atoms, molecules, and solids with atomic spatial resolution, allowing us to directly observe phenomena such as electron tunneling or electron-electron interaction in strong laser fields of few-cycle laser pulses.

DOI: 10.1103/PhysRevLett.123.203202

In recent years, attosecond science has revolutionized the fields of time-resolved spectroscopy and imaging [1–3]. Using attosecond pulses of electromagnetic radiation in an extreme ultraviolet (XUV) spectral region, electronic dynamics in various physical systems can be observed directly in the time domain [4,5]. However, direct imaging with atomic spatial resolution is not possible due to the wavelength of XUV photons, which is approximately hundred times larger than the interatomic distances. This limitation is removed when employing electrons with picometer de Broglie wavelengths for probing ultrafast dynamics via ultrafast electron diffraction or microscopy [6–11]. Temporal resolution of free electron-based imaging techniques is limited by the shortest achievable duration of electron pulses. Because of the dispersion of electron propagation velocity in vacuum, the shortest pulses generated directly by photoemission and static acceleration (without any additional compression) have durations of the order of 100 fs or more [12–14] allowing us to observe atomic motion, but the electronic dynamics occurring on attosecond timescales is not accessible.

Compression of freely propagating electron pulses via their interaction with optical fields has recently enabled reaching subfemtosecond electron pulse durations [15–17]. The longitudinal component of electron momentum can be modulated at optical frequencies either via the interaction with optical near fields of various nanostructures [18–20], longitudinal field inhomogeneity at thin dielectric or metallic films [15,16,21,22], or via ponderomotive interaction with an optical traveling wave [17,23–25]. After a drift distance, the longitudinal momentum modulation transfers to a density modulation due to dispersion of the electron group velocity in vacuum, and pulses with durations of several hundreds of attoseconds are formed [15–17]. In all of the compression schemes, the initial electron pulse duration is typically longer than the longitudinal modulation period and an attosecond electron pulse train with equidistant pulses is formed. Generation of isolated attosecond electron pulses via two-stage compression with the first stage based on radio frequency (rf) or THz cavity and the second stage driven by optical fields have been proposed [16,17,26]. However, the two-stage compression is technically challenging and the generation of isolated attosecond electron pulses using this technique has not been realized hitherto.

In this Letter we introduce an all-optical scheme, which allows us to directly select one of the attosecond pulses from the generated pulse train for time-resolved experiments. The principle is based on a synchronous ponderomotive interaction between the electrons and optical traveling waves formed by three laser pulses at different frequencies. The interaction introduces simultaneously a high frequency modulation of the electron energy or longitudinal momentum and a low-frequency transverse momentum modulation. The individual pulses in the electron pulse train are displaced in the transverse direction by a distance, which is larger than the electron beam diameter and spatial filtering by an aperture leads to selection of a single electron pulse from the train.

The layout of the proposed scheme is shown in Fig. 1(a). The electron pulse propagates horizontally and passes through the foci of three laser beams intersecting the electron beam under specific angles of incidence α, β, and γ. Polarizations of all three laser pulses are linear and point in the direction perpendicular to the plane of incidence (along the y coordinate).

The resulting light intensity distribution can be decomposed into three components, whose effect on the electron beam can be treated independently. The first synchronous

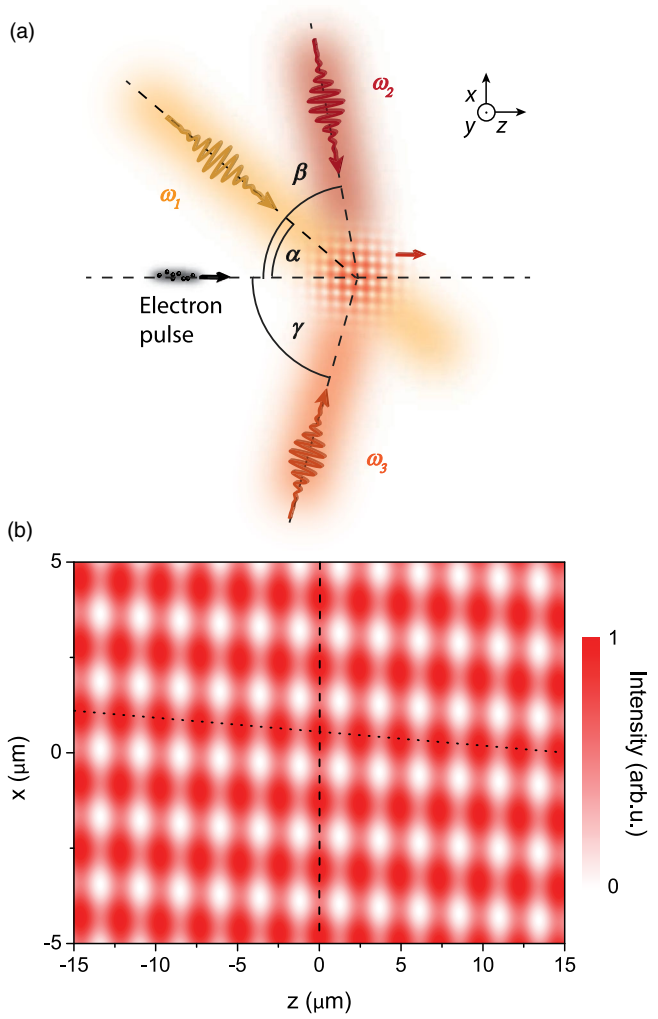

FIG. 1. (a) Layout of the proposed experimental setup for generation of isolated attosecond electron pulses. Three laser pulses at different frequencies ω_1, ω_2, and ω_3 are intersected with a pulsed electron beam traveling in z direction under angles α, β, and γ. (b) The intensity distribution of the synchronous optical traveling waves copropagating with the electrons given by Eq. (4). Dashed and dotted lines indicate the maxima of the intensity modulation in the longitudinal and the transverse directions, respectively.

traveling wave (its propagation velocity equals to the electron initial velocity) is generated by the beams at frequencies ω_1 and ω_2. The frequencies ω_1 and ω_2 and angles of incidence α and β are such that the energy and momentum conservation laws are fulfilled for purely longitudinal momentum modulation of the electrons (in the direction of the electron beam propagation) [25]. This can be expressed by the conditions

$$\omega_1 \sin\alpha = \omega_2 \sin\beta,$$
$$\cos\beta \cong \frac{(\beta_0 - \beta_0^{-1})\omega_1^2 - (\beta_0 + \beta_0^{-1})\omega_2^2 + 2\omega_1\omega_2\beta_0^{-1}}{2\omega_2(\omega_1 - \omega_2)}, \tag{1}$$

where β_0 is the electron initial velocity in units of speed of light c. The second term of Eq. (1) is obtained from Ref. [25] by assuming $2\hbar(\omega_1 - \omega_2)\Gamma/[m_0c^2(\Gamma^2 - 1)] \ll 1$, where $\Gamma = \sqrt{1 - \beta_0^{2-1}}$.

The second synchronous traveling wave, which serves for transverse streaking at lower frequency, is produced by the beams at frequencies ω_2 and ω_3, where $|\omega_3 - \omega_2| \ll |\omega_1 - \omega_2|$. The angle of incidence of the third beam γ is chosen to reach the synchronicity between the propagation velocity of the second optical traveling wave and the electron velocity as

$$\cos\gamma = \frac{\omega_2\cos\beta - (\omega_2 - \omega_3)\beta_0^{-1}}{\omega_3}. \tag{2}$$

However, the condition for purely longitudinal momentum transfer is not fulfilled here leading to a transverse force dependent on the electron injection phase. The third wave produced by the beams at frequencies ω_1 and ω_3 is not synchronous with the electrons and the momentum change of the electrons averages to zero over the time of the interaction. The snapshot of the intensity distribution of the two synchronous optical traveling waves propagating in the z direction in time $t = 0$ is shown in Fig. 1(b).

To obtain an analytical formula for the ponderomotive potential of the two synchronous waves in the electron rest frame we write the electric field of the three light beams intersecting with the electron beam under angles α, β, and γ as

$$\mathbf{E}_1(x,z,t) = \hat{\mathbf{y}}E_{10}\cos\left(\omega_1 t - \frac{\omega_1 z\cos\alpha}{c} + \frac{\omega_1 x\sin\alpha}{c} + \varphi_1\right),$$
$$\mathbf{E}_2(x,z,t) = \hat{\mathbf{y}}E_{20}\cos\left(\omega_2 t - \frac{\omega_2 z\cos\beta}{c} + \frac{\omega_2 x\sin\beta}{c}\right),$$
$$\mathbf{E}_3(x,z,t) = \hat{\mathbf{y}}E_{30}\cos\left(\omega_3 t - \frac{\omega_3 z\cos\gamma}{c} - \frac{\omega_3 x\sin\gamma}{c}\right), \tag{3}$$

where E_{10}, E_{20}, and E_{30} are electric field amplitudes of the individual beams, $\hat{\mathbf{y}}$ is the unit vector in the y direction, and φ_1 is the initial phase shift of the first wave. Ponderomotive potential in the subrelativistic interaction regime [$\Gamma \approx 1$ and $a_0 = eE_0/(m_0c\omega) \ll 1$, where e is the electron charge and m_0 is the electron rest mass] can be expressed as $U_\mathrm{p} = [e^2/(4m_0\omega^2)]|E|^2 = [e^2/(2m_0\omega^2\varepsilon_0 c)]I$. The ponderomotive force acting on the electrons is then $\mathbf{F}_\mathrm{p} = -\nabla U_\mathrm{p}$. The distribution of light intensity of the synchronous wave in the coordinate system traveling at the initial electron velocity β_0 obtained from the set of Eqs. (3) (when omitting constant terms that do not contribute to the ponderomotive force) can be written as

$$I(x',z') \approx E_{10}E_{20}\cos\left(\frac{(\omega_1\cos\alpha-\omega_2\cos\beta)}{c}z'+\varphi_1\right) + E_{20}E_{30}\cos\left(\frac{(\omega_3\cos\gamma-\omega_2\cos\beta)}{c}z'+\frac{(\omega_2\sin\beta+\omega_3\sin\gamma)}{c}x'\right), \tag{4}$$

where $z'=z-c\beta_0 t$ and $x'=x$. The angles of incidence α, β, and γ are given by Eqs. (1) and (2). The distribution of the transverse and the longitudinal components of the force acting on the electrons are obtained as spatial derivatives of Eq. (4) as

$$F_{\mathrm{T}} \approx -\frac{\partial I}{\partial z'} \approx E_{01}E_{02}\frac{(\omega_1\cos\alpha-\omega_2\cos\beta)}{c}\sin\left(\frac{(\omega_1\cos\alpha-\omega_2\cos\beta)}{c}z'+\varphi_1\right),$$
$$F_{\mathrm{L}} \approx -\frac{\partial I}{\partial x'} \approx E_{02}E_{03}\frac{(\omega_2\sin\beta+\omega_3\sin\gamma)}{c}\sin\left(\frac{(\omega_3\cos\gamma-\omega_2\cos\beta)}{c}z'+\frac{(\omega_2\sin\beta+\omega_3\sin\gamma)}{c}x'\right). \tag{5}$$

Here we neglect the second term of the longitudinal force coming from Eq. (4), which is small compared to the first term (condition $|\omega_3-\omega_2|\ll|\omega_1-\omega_2|$ is applied). The phase of the transverse momentum modulation occurring at frequency $\omega_{\mathrm{T}}=\omega_3-\omega_2$ depends both on the transverse and the longitudinal electron coordinates. Therefore it is necessary to perform the interaction in the focus of the electron beam, where the transverse beam size w_e is much smaller than the spatial period of the transverse momentum modulation $\Lambda_T=2\pi c/(\omega_2\sin\beta+\omega_3\sin\gamma)$. In this case, the resulting deflection angle of the electrons depends only on the initial longitudinal position of the electron in the electrons' rest frame z' and the phase of the optical traveling wave.

The resulting electron velocity change is calculated from the ponderomotive potential by integrating the classical equation of motion over the time of the interaction using impulse approximation. We note that we neglect quantum effects due to the fact that the temporal period of the longitudinal momentum modulation is larger than a typical temporal coherence time of the electron beam (<10 fs). This condition is equivalent to $\hbar\omega_1-\hbar\omega_2<\sigma_E$, where σ_E is the initial energy spread of the electron beam related to its coherence time via $\xi_t=\hbar/\sigma_E$ [27]. As a result we obtain the velocity change of the electron with an initial coordinate $z'\approx 0$ after the interaction as a function of the initial electron coordinates x' and z' as

$$\Delta\dot{z}' = \frac{e^2\tau_{\mathrm{eff}}E_{10}E_{20}}{4m_0^2\omega^2}\frac{(\omega_1\cos\alpha-\omega_2\cos\beta)}{c}\sin\left(\frac{(\omega_1\cos\alpha-\omega_2\cos\beta)}{c}z'+\varphi_1\right),$$
$$\Delta\dot{x}' = \frac{e^2\tau_{\mathrm{eff}}E_{20}E_{30}}{4m_0^2\omega^2}\frac{(\omega_2\sin\beta+\omega_3\sin\gamma)}{c}\sin\left(\frac{(\omega_3\cos\gamma-\omega_2\cos\beta)}{c}z'+\frac{(\omega_2\sin\beta+\omega_3\sin\gamma)}{c}x'\right). \tag{6}$$

Here $\tau_{\mathrm{eff}}=\tau_{\mathrm{FWHM}}w_{0z}\sqrt{\pi/(4\ln 2w_{0z}^2+2c^2\beta_0^2\tau_{\mathrm{FWHM}}^2)}$ is an effective interaction time given by the spatiotemporal overlap between the electron and the three optical waves, τ_{FWHM} is the pulse duration (full width at half maximum) of each pulse, w_{0z} is an average value of the $1/e^2$ radius of the laser beams in the z direction and $\omega=(\omega_1+\omega_2)/2$ is the effective value of the frequency for evaluation of the ponderomotive force (here we assume that $(\omega_1-\omega_2)/\omega\ll 1$). Propagation distance between the interaction and the temporal focus can be obtained from the derivative of the change of the longitudinal velocity component as

$$f_t = -\left(\left.\frac{d(\Delta\dot{z}')}{dz'}\right|_{z'=0}\right)^{-1}c\beta_0 = \frac{4m_0^2\omega^2c^3\beta_0}{e^2\tau_{\mathrm{eff}}E_{10}E_{20}(\omega_1\cos\alpha-\omega_2\cos\beta)^2}. \tag{7}$$

We note that for the fields given by Eq. (1), the negative sign of the derivative of the velocity change (electron velocity decreases with increasing z') required for electron compression in the center of the electron pulse $z'=0$ is obtained with the initial phase of the first wave $\varphi_1=\pi$.

To allow isolation of an individual attosecond electron pulse from the pulse train by spatial filtering using an aperture, the initial electron pulse duration has to be smaller than the temporal period of the transverse streaking by the second traveling wave $T_{\mathrm{T}}=2\pi/|\omega_2-\omega_3|$ and the streaking has to be strong enough to displace the subsequent electron pulses in the train by a distance, which is larger than the transverse size of the electron beam in the temporal focus $w_e(f_t)$. This gives a condition for the minimum ratio between the field amplitudes of the third and the first waves E_{30} and E_{10}:

$$\frac{E_{30}}{E_{10}}\frac{2\pi c(\omega_2\sin\beta+\omega_3\sin\gamma)(\omega_3\cos\gamma-\omega_2\cos\beta)}{(\omega_1-\omega_2)^2(\omega_1\cos\alpha-\omega_2\cos\beta)} > w_{\mathrm{e}}(f_t). \tag{8}$$

TABLE I. Parameters used in numerical simulations.

Laser beams	ω_1	ω_2	ω_3
Wavelength [nm]	1888	2266	2300
E_0 [V/m]	1.4×10^9	1.7×10^{10}	8×10^9
w_0 [μm]	15	15	15
τ_{FWHM} [fs]	300	300	300
Angle of incidence [°]	40.7	51.5	52.4

Electron beam				
E_k [keV]	σ_E [eV]	w_e [nm]	τ_{FWHM} [fs]	ε_T [pm rad]
200	0.5	15	200	3

The feasibility of the proposed approach is tested by numerical simulations of the interaction between the pulsed electron beam with a central kinetic energy of $E_k = 200$ keV and three light pulses. The electron energy is chosen due to the availability of ultrafast electron microscope-based sources of femtosecond single-electron pulses in this energy region [14]. However, the proposed scheme is universal and works in a wide range of initial electron energies up to ≈1 MeV. At higher electron energies, the initial energy spread of the electrons becomes comparable to the amplitude of the energy modulation, which can be introduced by laser pulses with realistic pulse energies. We solve the classical relativistic equation of motion with Lorentz force $(d/dt)(\Gamma m_0 \mathbf{v}) = q(\mathbf{E} + \mathbf{v} \times \mathbf{B})$ using the fifth-order Runge-Kutta algorithm. Laser fields are treated as Gaussian in both the transverse and the longitudinal directions with respect to their propagation direction with the polarization along the y direction perpendicular to the plane of incidence.

Initial electron distribution is assumed to be Gaussian with the transverse size of the beam in the focus $w_e = 15$ nm and the pulse duration of $\tau_{\mathrm{FWHM}} = 200$ fs. The energy spread of the electrons is $\sigma_E = 0.5$ eV (FWHM) and the normalized transverse emittance is $\varepsilon_T = 3$ pm rad (emittance of the diffraction-limited electron beam can be estimated as $\varepsilon_T = \beta_0 \Gamma \lambda_{dB}/(4\pi) \approx 0.2$ pm rad). All simulation parameters can be found in Table I. The practical limits for the electron beam spot size and emittance are $w_e < 50$ nm and $\varepsilon_T < 10$ pm rad for the set of laser parameters used. With larger values of w_e and ε_T, the beam diameter in the temporal focus becomes comparable to the transverse distance between two subsequent pulses in the train.

In Fig. 2(a) we show the distribution of the electron's transverse and longitudinal velocities immediately after the interaction with the laser fields. The spatial distribution of the electrons in the temporal focus after a drift distance of $f_t = 1.55$ cm is shown in Fig. 2(b) (the inset shows the detail of the central electron pulse). The diameter of the aperture $d = 16$ μm, which is used for spatial filtering of the electrons to obtain an isolated electron pulse, is indicated by dashed lines. The temporal profile of the

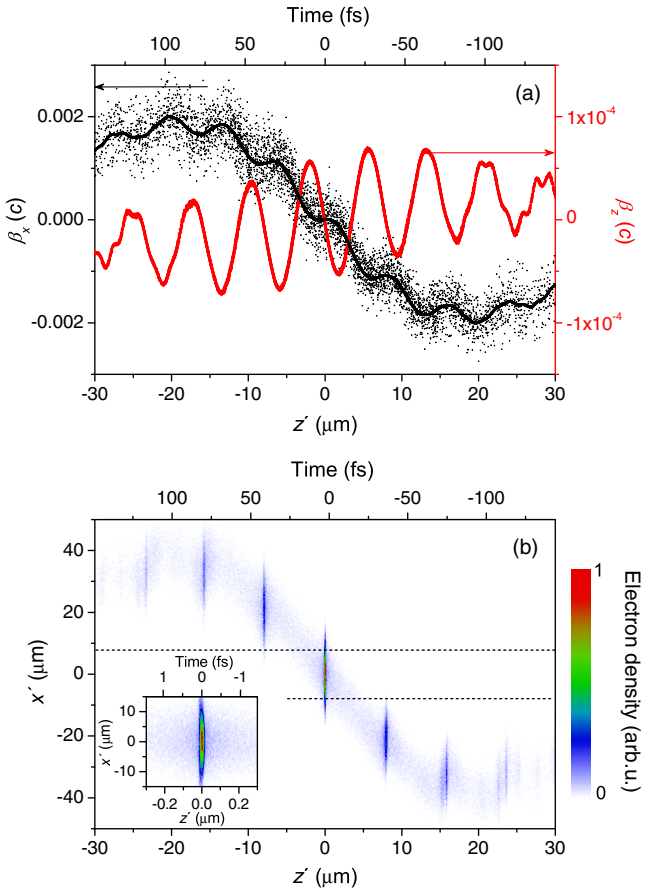

FIG. 2. (a) Distribution of the transverse (β_x, black points) and longitudinal (β_z, red points) velocity components of the electrons immediately after the interaction with the three laser pulses. Black curve corresponds to the center of the β_x distribution broadened due to electron beam divergence. (b) Spatial distribution of the electrons in the temporal focus after a drift distance of $f_t = 1.55$ cm downstream the interaction. The inset shows the detail of the central attosecond electron pulse.

electrons transmitted through the aperture shown in Fig. 3 reveals a pulse with a duration of $\tau_{e,\mathrm{FWHM}} = 90$ as. The minimum duration of the compressed electron pulse is limited by the initial uncorrelated energy spread of the electron beam and by the width of the electron energy spectrum after the interaction with optical fields, which is shown in the left inset of Fig. 3. The final energy spread of the compressed pulse is $\sigma_{E,\mathrm{fin}} = 73$ eV (relative energy spread $\sigma_{E,\mathrm{fin}}/E_k = 3.6 \times 10^{-3}$). Assuming conservation of the longitudinal phase-space volume, the minimum duration of the compressed electron pulse can be estimated as $\tau_{\mathrm{e,fin}} = \tau_{\mathrm{e,in}} \sigma_{E,\mathrm{in}}/\sigma_{E,\mathrm{fin}} = 65$ as. Here $\tau_{\mathrm{e,in}} = T_{\mathrm{L}}/4 = 0.5\pi/(\omega_1 - \omega_2)$ is the duration of one quarter of the period of the longitudinal velocity modulation determining the time window, in which the longitudinal velocity chirp introduced to the electrons by the ponderomotive interaction is approximately linear. We note that taking quantum effects into account would not change the result

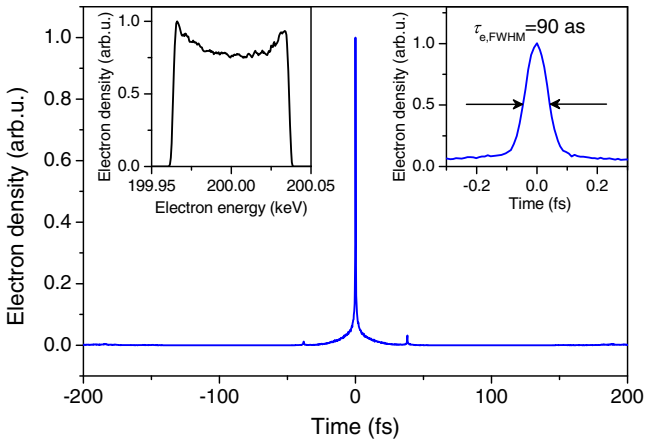

FIG. 3. Temporal profile of the electron density transmitted through an aperture with a diameter of $d = 16\ \mu$m [indicated by dashed lines in Fig. 2(b)]. Right inset shows the detail of the attosecond pulse with a duration of $\tau_{e,\mathrm{FWHM}} = 90$ as. Left inset shows the energy spectrum of the central attosecond electron pulse.

significantly as the minimum pulse duration obtained using quantum-mechanical considerations can be estimated as $\tau_{\mathrm{e,fin}}^{\mathrm{q-m}} \cong 25$ as [calculated using Eq. (3) in [28]].

The frequencies, which are used in numerical simulations, can be obtained from a single optical parametric amplifier (OPA) pumped by an ytterbium-doped solid state laser emitting at a wavelength of $\lambda = 1030$ nm. This technology allows generation of laser pulses with both high pulse energy and high repetition rate (the maximum pulse energy used in the numerical simulations is 40 μJ, which can be obtained with repetition rate $f_r > 100$ kHz). This is a necessary prerequisite for ultrafast imaging experiments with single-electron pulses because for formation of a single diffraction image, 10^5–10^7 electrons are required. Because the difference $\omega_3 - \omega_2$ is small, the two pulses at frequencies ω_2 and ω_3 can be obtained from a single pulse by splitting its spectrum.

For reaching attosecond timing control of the electrons, phase stability between the three laser pulses is required. This can be achieved either by using a carrier-envelope phase (CEP) stabilized laser system or by passive CEP stabilization of the idler beam in an OPA. The jitter of the arrival time of the isolated electron pulse is given by the stability of the difference between optical phases of the two laser pulses at frequencies ω_1 and ω_2 as $\Delta\tau = \Delta(\varphi_1 - \varphi_2)T_{\mathrm{L}}$. With the state-of-the-art performance, the CEP fluctuations of 100 mrad [29] are translated to a timing jitter of the attosecond electron pulse of ≈500 as (depending on the longitudinal modulation frequency ω_L), which is a much lower value than the best experimentally demonstrated timing stability for rf (≈10 fs [30]) or THz (≈3 fs [26]) compression schemes.

We note that the proposed technique is based on compression and filtering of the initial electron distribution and the total amount of electrons in the isolated attosecond pulse available for experiments is related to the initial pulse duration and the pulse charge. For the numerical simulations presented in this paper, the isolated attosecond pulse contains ≈5% of the charge of the initial electron pulse (within the time window of 1 fs). Because of the sinusoidal shape of the compression fields, there is a small background of uncompressed electrons from the central cycle of the traveling wave, which is partially filtered out by the aperture.

The application of periodic electron pulse trains is limited to investigation of cycle-reversible processes such as nonlinear electronic polarization in nanostructures or phase-resolved imaging of optical and plasmonic near fields. In contrast, the isolated attosecond electron pulses can serve for the study of processes, which are driven by few-cycle laser pulses and are not repetitive with the light cycle. These include, e.g., all the processes, where the electrons populate a real quantum state in the system already during the interaction with few-cycle light. Subcycle temporal resolution will enable us to study the effects of Coulomb interaction occurring during strong-field photoexcitation of high density electrons in solids, electron-electron, and electron-phonon scattering of high-energy quasiparticles accelerated by the strong light field or plasmonic damping in metallic nanostructures. Further, a direct cycle-resolved imaging of the electromagnetic fields generated during quantum tunneling of the electron wave packets from surfaces of nanostructures may become possible. The presented technique thus will lead to the extension of attosecond science to the field of high-resolution imaging using pulsed electron beams. Ponderomotive interaction with multiple laser beams combined with femtosecond pulse- and beam-shaping techniques also offers a more general framework and can be applied for electron wave packet shaping in quantum electron microscopy or for preparation of a certain spatiotemporal distribution of plasma density in laser-wakefield acceleration experiments.

The research was supported by Charles University (Center of Nano- and Bio-photonics, UNCE/SCI/010 and Project No. PRIMUS/19/SCI/05) and by Czech Science Foundation (Project No. 18-10486Y).

*Corresponding author.
kozak@karlov.mff.cuni.cz

[1] P. M. Paul, E. S. Toma, P. Breger, G. Mullot, F. Augé, Ph. Balcou, H. G. Muller, and P. Agostini, Science **292**, 1689 (2001).

[2] M. Hentschel, R. Kienberger, Ch. Spielmann, G. A. Reider, N. Milosevic, T. Brabec, P. Corkum, U. Heinzmann, M. Drescher, and F. Krausz, Nature (London) **414**, 509 (2001).

[3] G. Sansone, E. Benedetti, F. Calegari, C. Vozzi, L. Avaldi, R. Flammini, L. Poletto, P. Villoresi, C. Altucci, R. Velotta,

S. Stagira, S. De Silvestri, and M. Nisoli, Science **314**, 443 (2006).
[4] P. B. Corkum and F. Krausz, Nat. Phys. **3**, 381 (2007).
[5] M. Lucchini, S. A. Sato, A. Ludwig, J. Herrmann, M. Volkov, L. Kasmi, Y. Shinohara, K. Yabana, L. Gallmann, and U. Keller, Science **353**, 916 (2016).
[6] H. Ihee, V. A. Lobastov, U. M. Gomez, B. M. Goodson, R. Srinivasan, Ch.-Y. Ruan, and A. H. Zewail, Science **291**, 458 (2001).
[7] R. Srinivasan, J. S. Feenstra, S. T. Park, S. J. Xu, and A. H. Zewail, Science **307**, 558 (2005).
[8] M. Gao, Ch. Lu, H. Jean-Ruel, L. Ch. Liu, A. Marx, K. Onda, S. Koshihara, Y. Nakano, X. Shao, T. Hiramatsu, G. Saito, H. Yamochi, R. R. Cooney, G. Moriena, G. Sciaini, and R. J. D. Miller, Nature (London) **496**, 343 (2013).
[9] B. J. Siwick, J. R. Dwyer, R. E. Jordan, and R. J. D. Miller, Science **302**, 1382 (2003).
[10] P. Baum, D. S. Yang, and A. H. Zewail, Science **318**, 788 (2007).
[11] H. S. Park, J. S. Baskin, and A. H. Zewail, Nano Lett. **10**, 3796 (2010).
[12] M. Aidelsburger, F. O. Kirchner, F. Krausz, and P. Baum, Proc. Natl. Acad. Sci. U.S.A. **107**, 19714 (2010).
[13] J. Hoffrogge, J. P. Stein, M. Krüger, M. Förster, J. Hammer, D. Ehberger, P. Baum, and P. Hommelhoff, J. Appl. Phys. **115**, 094506 (2014).
[14] A. Feist, N. Bach, N. R. da Silva, T. Danz, M. Möller, K. E. Priebe, T. Domröse, J. G. Gatzmann, S. Rost, J. Schauss, S. Strauch, R. Bormann, M. Sivis, S. Schäfer, and C. Ropers, Ultramicroscopy **176**, 63 (2017).
[15] K. E. Priebe, C. Rathje, S. V. Yalunin, T. Hohage, A. Feist, S. Schäfer, and C. Ropers, Nat. Photonics **11**, 793 (2017).
[16] Y. Morimoto and P. Baum, Nat. Phys. **14**, 252 (2018).
[17] M. Kozák, N. Schönenberger, and P. Hommelhoff, Phys. Rev. Lett. **120**, 103203 (2018).
[18] A. Feist, K. E. Echternkamp, J. Schauss, S. V. Yalunin, S. Schäfer, and C. Ropers, Nature (London) **521**, 200 (2015).
[19] K. E. Echternkamp, A. Feist, S. Schäfer, and C. Ropers, Nat. Phys. **12**, 1000 (2016).
[20] M. Kozák, J. McNeur, K. J. Leedle, H. Deng, N. Schönenberger, A. Ruehl, I. Hartl, J. S. Harris, R. L. Byer, and P. Hommelhoff, Nat. Commun. **8**, 14342 (2017).
[21] Y. Morimoto and P. Baum, Phys. Rev. A **97**, 033815 (2018).
[22] F. O. Kirchner, A. Gliserin, F. Krausz, and P. Baum, Nat. Photonics **8**, 52 (2014).
[23] P. Baum and A. H. Zewail, Proc. Natl. Acad. Sci. U.S.A. **104**, 18409 (2007).
[24] S. A. Hilbert, C. Uiterwaal, B. Barwick, H. Batelaan, and A. H. Zewail, Proc. Natl. Acad. Sci. U.S.A. **106**, 10558 (2009).
[25] M. Kozák, T. Eckstein, N. Schönenberger, and P. Hommelhoff, Nat. Phys. **14**, 121 (2018).
[26] C. Kealhofer, W. Schneider, D. Ehberger, A. Ryabov, F. Krausz, and P. Baum, Science **352**, 429 (2016).
[27] P. Baum, Chem. Phys. **423**, 55 (2013).
[28] P. Baum, J. Appl. Phys. **122**, 223105 (2017).
[29] T. Balčiūnas, T. Flöry, A. Baltuška, T. Stanislauskas, R. Antipenkov, A. Varanavičius, and G. Steinmeyer, Opt. Lett. **39**, 1669 (2014).
[30] A. Gliserin, M. Walbran, F. Krausz, and P. Baum, Nat. Commun. **6**, 8723 (2015).